SAND REPORT
SAND2005-5935
Unlimited Release
Printed September 2005

Advancements in Sensing and Perception using Structured Lighting Techniques: An LDRD Final Report

Denise D. Padilla, Patrick A. Davidson Jr., Jeffrey J. Carlson, David K. Novick

Prepared by
Sandia National Laboratories
Albuquerque, New Mexico 87185 and Livermore, California 94550

Sandia is a multiprogram laboratory operated by Sandia Corporation, a Lockheed Martin Company, for the United States Department of Energy under Contract DE-AC04-94AL85000.

Sandia National Laboratories

Issued by Sandia National Laboratories, operated for the United States Department of Energy by Sandia Corporation.

Available to DOE and DOE contractors from
U.S. Department of Energy
Office of Scientific and Technical Information
P.O. Box 62
Oak Ridge, TN 37831

Telephone: (865)576-8401
Facsimile: (865)576-5728
E-Mail: reports@adonis.osti.gov
Online ordering: http://www.doe.gov/bridge

Available to the public from
U.S. Department of Commerce
National Technical Information Service
5285 Port Royal Rd
Springfield, VA 22161

Telephone: (800)553-6847
Facsimile: (703)605-6900
E-Mail: orders@ntis.fedworld.gov
Online order: http://www.ntis.gov/ordering.htm

SAND2005-5935
Unlimited Release
Printed September 2005

Advancements in Sensing and Perception using Structured Lighting Techniques: An LDRD Final Report

Denise D. Padilla
Patrick A. Davidson Jr.
Jeffrey J. Carlson
David K. Novick

Intelligent Systems and Robotics Center

Sandia National Laboratories
P.O. Box 5800
Albuquerque, NM 87185-1003

Abstract

This report summarizes the analytical and experimental efforts for the Laboratory Directed Research and Development (LDRD) project entitled "Advancements in Sensing and Perception using Structured Lighting Techniques". There is an ever-increasing need for robust, autonomous ground vehicles for counter-terrorism and defense missions. Although there has been nearly 30 years of government-sponsored research, it is undisputed that significant advancements in sensing and perception are necessary. We developed an innovative, advanced sensing technology for national security missions serving the Department of Energy, the Department of Defense, and other government agencies. The principal goal of this project was to develop an *eye-safe*, robust, low-cost, lightweight, 3D structured lighting sensor for use in broad daylight outdoor applications. The market for this technology is wide open due to the unavailability of such a sensor. Currently available laser scanners are slow, bulky and heavy, expensive, fragile, short-range, sensitive to vibration (highly problematic for moving platforms), and unreliable for outdoor use in bright sunlight conditions. Eye-safety issues are a primary concern for currently available laser-based sensors. Passive, stereo-imaging sensors are available for 3D sensing but suffer from several limitations: computationally intensive, require a lighted environment (natural or man-made light source), and don't work for many scenes or regions lacking texture or with ambiguous texture. Our approach leveraged from the advanced capabilities of modern CCD camera technology and Center 6600's expertise in 3D world modeling, mapping, and analysis, using structured lighting. We have a diverse customer base for indoor mapping applications and this research extends our current technology's lifecycle and opens a new market base for outdoor 3D mapping. Applications include precision mapping, autonomous navigation, dexterous manipulation, surveillance and reconnaissance, part inspection, geometric modeling, laser-based 3D volumetric imaging, simultaneous localization and mapping (SLAM), aiding first responders, and supporting soldiers with helmet-mounted LADAR for 3D mapping in urban-environment scenarios. The technology developed in this LDRD overcomes the limitations of current laser-based 3D sensors and contributes to the realization of intelligent machine systems reducing manpower need.

Acknowledgements

The authors wish to thank the following individuals for their invaluable contributions, time, extensive discussions on the project, and input to this final report:

Arnold Augustoni, Department 1128

Chris Wilson, Department 6646

Dan Small, Department 6646

John Feddema, Department 6634

Chuck Duus, Department 6646

Mike Kuehl, Department 6634

Paul Johnson, Department 6632

Frank Gerdin, Department 6454

Table of Contents

List of Figures

List of Tables

Introduction

Since the terrorists acts of 9/11 there is an ever-increasing need for autonomously navigating vehicles for counter-terrorism, defense missions, and other military applications. The limiting factor in autonomous navigation is the ability to sense and perceive the environment. It is undisputed that significant advancements in sensing and perception are necessary. The principal goal of this project was to develop an innovative eye-safe, robust, low-cost, lightweight 3D structured lighting sensor for use in broad daylight outdoor applications. Structured lighting systems provide a way of mapping and modeling the environment in three-dimensions using a camera, laser, and a computer to process the data. The geometry of the system allows one to calculate the position of a point using triangulation. In addition, the laser light is projected in a precise pattern (grid, line, ellipse etc.), which allows surface shapes to be deduced from the distortion of the pattern on an object's surface. Structured lighting requires image processing to isolate, or segment, a laser signal from background clutter in a camera image. Segmenting the laser signal is easy if the reflected laser light is significantly brighter than the background clutter due to reflected ambient light. Under most outdoor conditions and some indoor conditions, however, reflected energy from background clutter is often significantly greater than the reflected laser energy. Problems also occur when the reflective surface is highly absorptive, such as asphalt. The market for this technology is wide open due to the unavailability of such a sensor. Currently available laser scanners are slow, bulky and heavy, expensive, fragile, sensitive to vibration (highly problematic for moving platforms), and unreliable for outdoor use in bright sunlight conditions. Eye-safety issues are a primary concern for currently available laser-based sensors. Robust solutions to these problems are needed in order to extend the practical application of laser-based 3D structured lighting vision systems. Passive, stereo-imaging sensors are available for 3D sensing but suffer from several limitations: computationally intensive, require a lighted environment (natural or man-made light source), and don't work for many scenes or regions lacking texture or with ambiguous texture. A small subset of possible applications include precision mapping, obstacle detection for autonomous navigation, dexterous manipulation, surveillance and reconnaissance, part inspection, geometric modeling, simultaneous localization and mapping (SLAM), and aiding first responders. The technology developed in this LDRD overcomes the limitations of current laser-based 3D sensors and can contribute to the realization of intelligent machine systems reducing manpower need.

Technical Approach

The following background suppression methods were investigated to maximize the signal to background clutter ratio:

- Utilizing a Naturally Blocked Laser Frequency in the H_2O Absorption Band
- Temporal Differencing
- Spatial Differencing
- Linear Polarization Imaging Methods
- Spectral Estimation
- Laser Pulsing

Naturally Blocked Laser Frequency

We investigated using a laser frequency within a narrow band centered at 1.392 μm where atmospheric constituents prevent nearly 100% of the sun's light from reaching the Earth's surface. However, this wavelength falls outside of the sensitivity range of a standard CCD (Charge-Coupled Device) camera requiring an expensive, bulky, short-wave IR camera. In addition, the absorption band at this wavelength is narrower than the bandwidth of available optical band-pass filters. To maximize the signal to noise ratio (SNR) while remaining eye-safe,

$$SNR_{\lambda} = \frac{(Power_{Laser})(CCD\ response_{\lambda})}{Solar\ Irradiance_{\lambda}}$$

we chose a laser with a wavelength of 830 nm and a continuous optical output power of 5mW. This output power is considered eye-safe under the ANSI standards. At this wavelength, H_2O and other atmospheric constituents block a significant amount of the sun's light. The spectral distribution curve below illustrates solar irradiance at various wavelengths and major absorption bands in the atmosphere are clearly apparent.

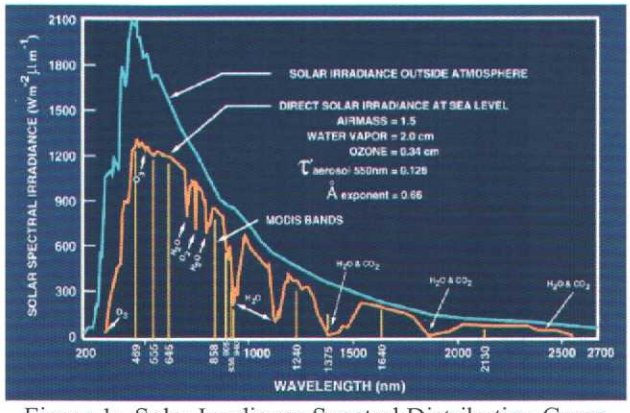

Figure 1: Solar Irradiance Spectral Distribution Curve

In addition, 830 nm falls within the sensitivity range of a standard silicon CCD (Charge-Coupled Device) camera. The spectral response curve for silicon CCD cameras is shown below.

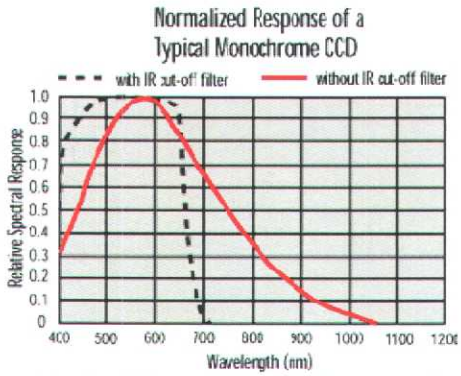

Figure 2: CCD Camera Spectral Response Curve

To further increase the signal to noise ratio, a 10 *nm* bandwidth optical band-pass filter centered at the laser wavelength was used. The filter is placed in front of the camera lens and blocks all reflected ambient light with wavelengths outside the pass band of the filter. Since the laser light is at the center of the pass band, it is readily passed by the filter and easily seen by the camera. Although this is the narrowest filter available at this wavelength, it was still too broad for background clutter suppression in bright sunlight conditions. Figure 3 illustrates that the laser spot cannot be isolated from background clutter with a filter alone. Increasing the laser power is one solution that leads to eye safety issues.

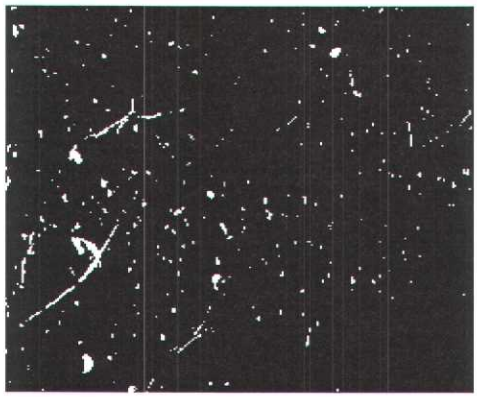

Figure 3: Thresholded Image of an 830 *nm* Filter Response with the Laser On

Temporal Differencing

Next, a temporal differencing method was implemented to extract the laser. This method subtracts two consecutive images, one with the laser on and the other with the laser off. First, the laser is turned on projecting the structured light pattern onto the scene and an image $I_1(x, y)$ is acquired and stored in computer memory. This image can be modeled as background B(x, y) plus laser signal S(x, y). The indices x and y are integer values representing the respective column and row position of each pixel in the image. In our application the pixel depth is 8 bits with values ranging from 0 to 255, 0 representing the darkest shade of grey (black) and 255 representing the lightest shade of grey (white). Next, the laser is turned off and another image $I_2(x, y)$, consisting of only background, is acquired. Assuming the ambient illumination is constant during the acquisition of both images, $I_2(x, y)$ can be modeled as background B(x, y). The difference, D(x, y), obtained by subtracting $I_2(x, y)$ from $I_1(x, y)$, suppresses the background clutter and reveals the structured light pattern.

$$\begin{aligned} D(x, y) &= I_1(x, y) - I_2(x, y) \\ &= B(x, y) + S(x, y) - B(x, y) \\ &= S(x, y) \end{aligned}$$

In the absence of noise, the differences are assumed to be exactly zero in the regions where both $I_1(x, y)$ and $I_2(x, y)$ contain only background, $B(x, y)$. Noise, resulting from electronic noise in the camera itself and from random variations in ambient illumination, generally results in small but measurable differences. Because these differences are generally symmetric about zero, a simple method for detecting, or segmenting, the laser signal is to compare the absolute value of $D(x, y)$ to a fixed threshold, T. Differences that exceed the threshold are marked as changed pixels indicating the presence of laser light.

Figure 4 shows the filter response with the laser on while Figure 5 is the response with the laser off. The mean grey level of the image with the laser on was calculated to be 140.5 and the standard deviation was 44.9. The grey level of the laser was 255 making the laser spot only ~2.56 standard deviations above the mean.

Figure 4: 830 *nm* Filter Response with the Laser On

Figure 5: 830 *nm* Filter Response with the Laser Off

Figure 6 is the simple difference image with a mean grey level of 3.28, a standard deviation of 3.42 and the laser grey level of 117. The laser spot is now ~33 standard deviations above the mean, a vast improvement. Figure 7 is the thresholded image with the threshold set to 107. The laser spot can be extracted from the image.

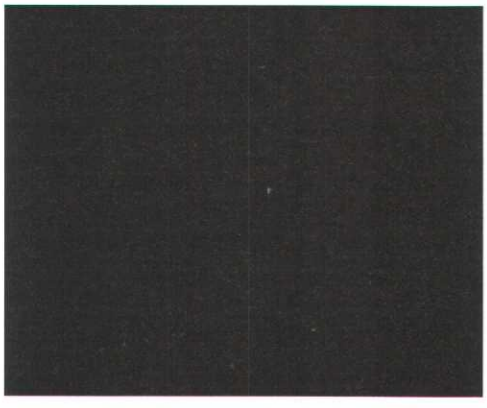

Figure 6: Difference Image

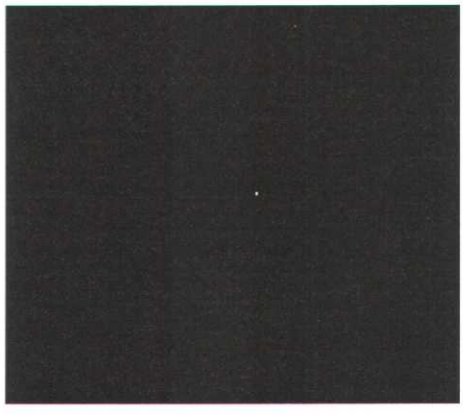

Figure 7: Threshold Image

Although this method has been used successfully for clutter suppression, it requires a stationary or expensive, high-speed camera. For example, at 5 ft/sec an object will move 2 inches in 1/30 sec (standard CCD frame rate). If the camera views a footprint on the ground of 4 feet by 3 feet, and has a pixel resolution of 640 x 480 pixels, then the physical resolution of the imaging system is approximately 13 pixels per inch. An object moving 2 inches would move by approximately 26 pixels in the image. This would result in significant differences detected in the segmentation process using temporal differencing.

Spatial Differencing

A spatial differencing method that uses a spatial band-pass filter to detect the laser was also implemented. In this method, pixels from two regions are used to estimate pixel values in another spatially proximate region. In this example, A, B, and C are pixel averages in three separate regions and regions A and C are used to estimate the pixel values in region B.

A
B
C

$$B_{est} = (A + C)/2$$

If $B - B_{est} \geq Thd$, then a bright spot from the laser has been detected. With this method the laser could not be isolated from the background clutter as can been seen in Figures 8 and 9.

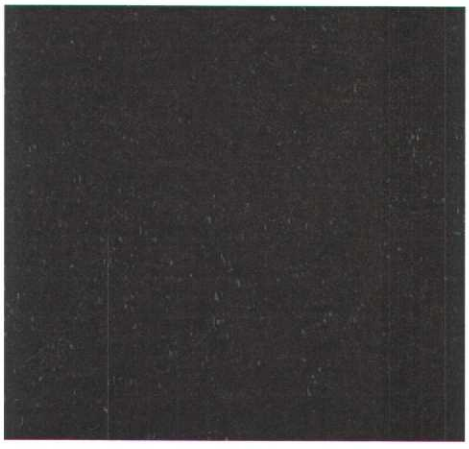

Figure 8: Spatial Differencing Image
Mean Grey Level = 16.61
Laser Grey Level = 82
Standard Deviation = 13.32
Laser spot is ~5 standard deviations above the mean

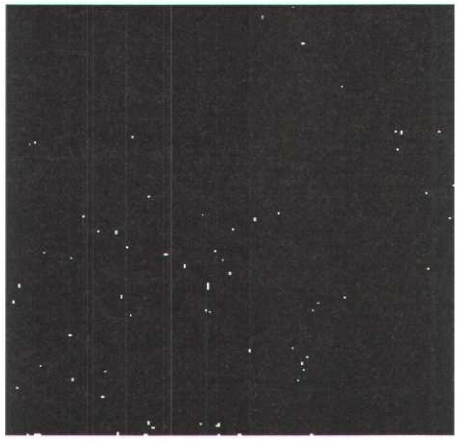

Figure 9: Thresholded Image
Threshold = 72

Linear Polarization Imaging Methods

Next, a polarization-sensitive system was implemented to increase the signal-to-clutter ratio. The kinds of surfaces that were imaged were natural and man-made, such as asphalt, concrete, dirt and grass. A series of measurements was made for each of the materials studied in order to find the best configuration for the polarizing system and also to find out the potential improvement in the signal to clutter ratio. This process was divided into three parts: characterization of the reflected sunlight, characterization of the reflected laser light, and measurement of the improvement in the signal to clutter ratio.

Theoretical Background

The polarization of light phenomenon is widely found in nature. Insects and octopus, for example, use this principle in their vision systems [1], [2]. It has been demonstrated that polarization properties of back-scattered light give more information of an imaged object than only the total intensity.

Three different phenomena produce changes in the polarization state of light when it reaches some material: scattering, diffraction and reflection. In this research we are particularly interested in reflection, since the signal measured by the detector is the diffuse reflected light and since all the materials to be tested are solid and opaque.

Most natural light, like sunlight, has a random polarization state. The unpolarized light usually becomes totally or partially linearly polarized when reflected by a surface. It will become circularly polarized only if the linearly polarized light subsequently passes through certain types of objects in specific situations. Because of this, circular polarization is not so common in nature. Unpolarized light when reflected by some surface will always be somewhat linearly polarized. The only cases in which there will be no polarization are when the light is totally reflected or when the angle of incidence is 90°. The degree of polarization of the reflected beam will vary basically according to the characteristics of the surface and the angle of incidence. The polarization degree is maximum at an incidence angle equal to Brewster's angle. [2]

Each kind of material produces a different polarization effect when it reflects unpolarized light. Unpolarized light becomes partially linearly horizontally polarized when reflected by a smooth non-metallic surface, and in favorable situations total polarization can result. In the case of rough surfaces the reflected light will be linearly polarized, but can have different orientations than horizontal. The degree of polarization is usually smaller than that produced by smooth surfaces, because of the multiple reflections in the irregularities of the material. According to the Umov Rule [3], the darker the object the stronger the polarization of its reflected light. Therefore, snow will polarize less than asphalt, for example. Also, the maximum degree of polarization is inversely proportional to the reflectivity of the material. The Umov Rule can be explained by the fact that in a dark material the light that is reflected due to the roughness of the surface loses its intensity due to the high absorption of the material. Therefore the reflected light that comes off of the material is basically reflected only one time and thus is polarized.

As in the case of unpolarized light, different materials also produce alterations in the pattern of the polarized light when submitted to reflection. It is possible that part of the linearly polarized incident light can become circularly polarized when total reflection takes place. This will happen for angles of incidence smaller than the Brewster angle and is directly related to the refractive index of the material. In some special situations it is possible that the linearly polarized light becomes totally circularly polarized, but the refractive index of the surface has to be very high, like in diamonds for example. A material with lower refraction index can produce circularly polarized light only if the light comes from a previous reflection. Therefore, it is not unrealistic to consider that in most cases of reflection of linearly polarized light, a linear component will still be observed.

Linearly polarized light when reflected by a non-metallic smooth surface still comes out polarized. The horizontal component is strongly reflected while the vertical component is weakened and becomes zero at the Brewster angle. For angles of incidence smaller than the Brewster angle, a mirror effect occurs and a shift of 90° in the polarization shows up in the reflected light. This happens because of a phase-shift of the vertically polarized component. However, this change has no effect on the horizontal component. Rough surfaces produce a depolarization when reflecting linearly polarized light. However, some of the original polarization still remains. The depolarization is stronger in bright surfaces than in dark ones (Umov's Law).

The materials intended to be studied were classified as rough surfaces: asphalt, concrete, dirt and grass. In some special situations like when they are wet, their characteristics can change and they can approximate a smooth surface.

As described above, linear polarization will take place when unpolarized light is reflected by the surface. The degree of polarization will be higher for asphalt than for concrete, for example, due to the Umov's Law. When polarized light reaches the surface it will be depolarized somewhat, but still a linear component will be reflected.

Based on these observations it is possible to conclude that an optical system can be designed to collect minimum intensity from reflected sunlight. In order to do this a polarizer is used, oriented at an angle that is orthogonal to the polarization angle of the reflected sunlight. Since the objective of this research is to reduce the clutter background from the sun it is desirable that in the worst situation (favorable angle of incidence and surface characteristics), the reflected linearly polarized sunlight will have a different (preferably orthogonal) angle than the reflected linearly polarized light due to the laser signal.

Methodology

The total intensity of light detected by a CCD camera can be defined as the sum of the horizontal and vertical intensity components:

$$I = I_H + I_V . \qquad (1)$$

If R is defined as the ratio between the horizontal and the vertical components, equation (1) can be written as:

$$I = (1+R)\times I_V , \qquad (2)$$

where:

$$R = \frac{I_H}{I_V} . \qquad (3)$$

If a vertically oriented polarizer is placed in front of the camera, the intensity of light detected will correspond only to the vertical component:

$$I_{pol} = I_V . \qquad (4)$$

The signal to clutter ratio (STC) in the imaging laser system described above is defined as:

$$STC = \frac{I_L}{I_S} , \qquad (5)$$

where:
I_L is equal to the laser light intensity detected by the camera;
I_S is equal to the sunlight intensity detected by the camera in the same area of the laser spot.

The improvement (IMP) in the signal to clutter ratio that can be obtained by using polarization in the system is defined by the ratio between the STC with a polarizer (STC_{pol}) and without the polarizer:

$$IMP = \frac{STC}{STC_{pol}} = \frac{\frac{I_{Vlaser}}{I_{Vsun}}}{\frac{(1+R_{laser})\times I_{Vlaser}}{(1+R_{sun})\times I_{Vsun}}}$$

$$IMP = \frac{1+R_{sun}}{1+R_{laser}} , \qquad (6)$$

where:
R_{sun} is the ratio between the horizontal and the vertical intensity components of the reflected sunlight;
R_{laser} is the ratio between the horizontal and the vertical intensity components of the reflected laser light;
I_{Vsun} is the intensity of the vertical component of the reflected sunlight;
I_{Vlaser} is the intensity of the vertical component of the reflected laser light.

Therefore, the improvement that can be achieved by placing a vertical polarizer in the field of view of the CCD camera depends only on R_{sun} and R_{laser}. For an IMP bigger than unity, R_{sun} has to be bigger than R_{laser}.

The same development can be done for any angle of polarization. A vertical polarizer was chosen because in all measurements the reflected sunlight was more horizontally oriented. Therefore, by using a vertical polarizer at the camera, the sunlight at the detector would be less intense than if a horizontal polarizer were used. In order to maximize the IMP, a vertically oriented laser is used. With this configuration the lowest R_{laser} is obtained.

The analysis of equation (6) brings out important information about the system. If, after reflecting on the surface, the sunlight remains totally unpolarized and the laser light is totally depolarized, R_{sun} and R_{laser} will be equal to unity. Therefore no improvement would be obtained with the use of polarizers. The maximum improvement would be reached if the reflected sunlight is totally horizontally oriented and the reflected laser light remains vertically polarized.

Optical Setup

The optical setup consisted of a 650 nm, 3 mW, CW laser; a 10 nm filter centered at 650 nm; a polarizer and a CCD camera with a resolution of 640 x 480, that is able to capture frames with a depth of 8 bits. The optical parts were fixed on a tray on the top of an adjustable tripod, which gives the necessary portability for outdoor use. The picture of the set up is seen below.

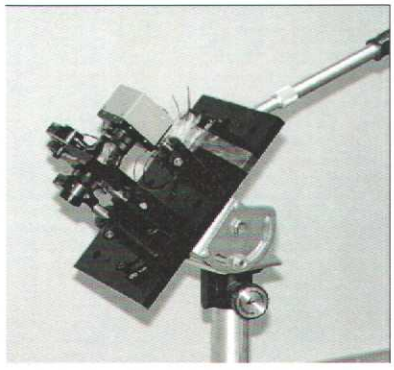

Figure 10: Optical Setup

Measurements

In order to define IMP, R_{sun} and R_{laser} should be measured for each one of the surfaces of interest. To measure R_{sun}, two frames were taken with the CCD camera – one with the polarizer vertically oriented and one with it horizontally oriented. Two cases were observed: one with the camera pointed to the ground (for asphalt, concrete, grass and dirt) at 45°, and the other one with the camera pointing to an obstacle in front of it at 90° (for the concrete wall). By dividing the average pixel values of these two frames (horizontal by vertical), R_{sun} is obtained. Since the R value depends on the sun's incidence angle, the measurements were taken at two different times during the day, the first one with the sun at 90° (minimum R), and the other one with the sun at a grazing angle, which corresponds to the maximum R [4]. Therefore, with these two limiting values it is possible to define the range of improvement in the STC. The values measured for R_{sun} for each of the surfaces are shown in the Table 1 below.

Surface	R_{sun} (90°)	R_{sun} (grazing angle)
Asphalt	1.14	1.81
Concrete	1.17	1.45
Dirt	1.05	1.23
Grass	1.19	1.41
Concrete wall	1.16	1.06

Table 1: Values of R_{sun}

Figure 11 presents the two frames taken for concrete with the sun at a grazing angle.

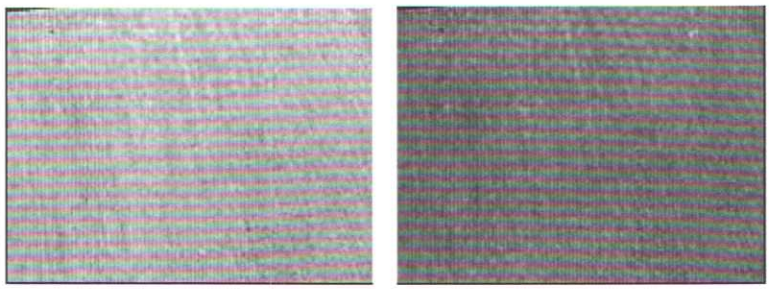

(a) (b)

Figure 11: Image of the concrete with a horizontal polarizer (a) and with a vertical polarizer (b)

The same procedure was used to measure R_{laser} with the exception that the measurements were taken at night in order to eliminate the clutter from the sun. In addition, the average pixel values were calculated only for the area corresponding to the laser spot. The values measured for R_{laser} for each of the surfaces are shown in Table 2 below.

Surface	R_{laser}
Asphalt	0.34
Concrete	0.56
Dirt	0.50
Grass	0.37
Concrete wall	0.66

Table 2: Values of R_{laser}

Figure 12 presents the two laser image frames taken for concrete.

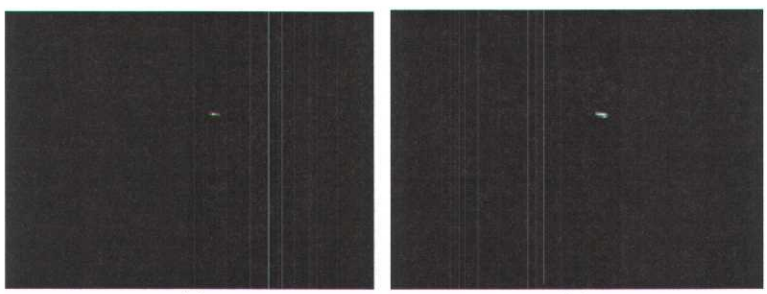

(a) (b)

Figure 12: Laser images of concrete with a horizontal polarizer (a) and with a vertical polarizer (b)

With the R_{sun} and R_{laser} values for each one of the surfaces, the improvement in the STC can be calculated. The results are presented in Table 3 below.

Surface	IMP (90°)	IMP (grazing angle)
Asphalt	1.60	2.10
Concrete	1.40	1.57
Dirt	1.37	1.49
Grass	1.60	1.76
Concrete wall	1.30	1.24

Table 3: Improvements in the signal to clutter ratio

To validate the values obtained in Table 3, another method was used to calculate them. The intention was to simulate the situation in which no polarizer is used and to compare the STC with the one obtained for a system with a vertical polarizer. To do this four frames were necessary, two with the laser on, and two with the laser off. With the laser on, one frame had the polarizer vertically oriented while the other frame had the polarizer horizontally oriented. The same procedure was done with the laser off. Again the measurements took place in two different times during the day for each one of the surfaces.

In order to simulate the STC that would be obtained with no polarizer, the vertical and horizontal frames with the laser on were added and the background signal was subtracted from it. Then the average intensity calculated in the laser spot area was divided by the average intensity calculated for the background. The background image was the one obtained by adding the vertical and horizontal components of the scene, taken with the laser off. Following this procedure the STC for a system with no polarizer was calculated.

To calculate the STC for a system with a vertical polarizer, the vertical image of the background only was subtracted from the vertical image with the laser on and the result was divided by the background. Figure 13 shows the two final frames obtained for concrete.

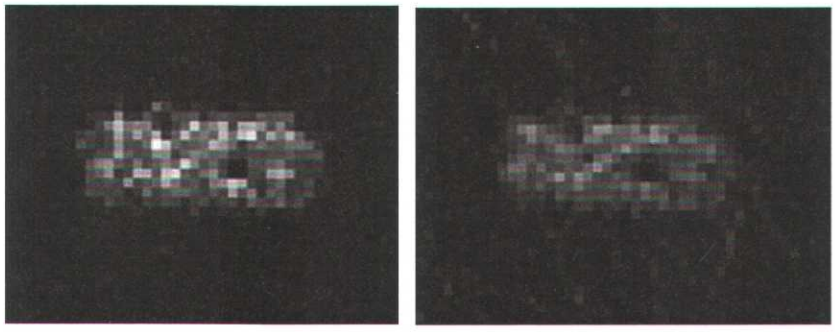

(a) (b)

Figure 13: Laser image on concrete using vertical polarization (a) and no polarization (b)

By dividing the STC's calculated for these two different situations the improvement in the system was calculated. Table 4 below shows the values obtained for each one of the surfaces.

Surface	IMP (90°)	IMP (grazing angle)
Asphalt	1.65	2.02
Concrete	1.32	1.61
Dirt	1.31	1.52
Grass	1.56	1.50
Concrete wall	1.20	1.15

Table 4: Improvements in the signal to clutter ratio using a simulating technique

All measurements were taken with clear sky, i.e. no clouds were blocking the sunlight. Also, the surfaces were dry.

Indoor measurements were also taken. The measurements were conducted in the same way as described above and the surfaces analyzed were synthetic floor, painted wall, and white cloth. The improvement values obtained using the two techniques described above are presented in the Table 5 below.

Surface	Measuring R	Simulation
Synthetic floor	1.04	1.02
Painted wall	1.06	1.03
White cloth	1.03	1.04

Table 5: Improvements in the signal to clutter ratio for an indoor application

The results show he imaging systems under analysis for outdoor use. By placing a vertical polarizer on the CCD camera it is possible to obtain improvements for concrete, dirt, grass, and a concrete wall. Although the STC improvements reached may not be sufficient to completely mitigate the background sunlight issue, the implementation of a polarizing system is a very simple and inexpensive upgrade to the system and can be used in combination with the other techniques studied. As expected, asphalt presented better results due to Umov's Law. For indoor applications, and considering the surfaces analyzed, the technique seems to have minimal effect. This is due to the fact that there is a large amount of depolarization in the reflected laser light and that the background light remains unpolarized after reflection.

The results show that by using polarization properties it is possible to design an outdoor optical system that is able to increase the signal to clutter ratio from approximately 30% to 100% in the imaging system, depending on the kind of surface and on the incidence angle of the sunlight.

Spectral Estimation

Next, we implemented a spectral estimation algorithm that has been demonstrated in audio systems, allowing the discrimination of one voice in a noisy background. This method is an interpolation between separate spectral bands to determine the presence of light in a neighboring band. The two bands are equally spaced outside the center band in order to estimate the center response. This technique exploits the fact that reflective properties of many manmade and natural surfaces do not vary much over narrow ranges of light frequency (i.e. over a narrow spectral band). When illuminated by a broadband source such as the sun, the energy of light reflected off of a surface over one narrow band is approximately the same as that reflected from another nearby, but separate, narrow band. The following equations describe how an estimated background image at the center band is created through linear interpolation of the neighboring bands.

$$\hat{Y}_{ij} = k_0 + k_1 X_{ij} + k_2 Z_{ij}$$

This is the general solution for the estimated image where $\hat{Y}$ is the image estimate, X is the lower spectral band response, and Z is the upper spectral band response. The coefficient k_0 represents the DC offset and k_1 and k_2 are the weights for each of the spectral responses on either side of the center response. The laser frequency falls within the middle of the center band and is outside the pass bands of the upper and lower spectral bands. The estimate is unable to closely approximate the laser signal due to the lack of correlation in the neighboring bands. Simple differencing between the actual response at the center band and the estimated image at the center band subtracts out the background clutter and allows easy segmentation of the laser. The following equation calculates the error between the estimated image $\hat{Y}$ and the actual image response Y.

$$e_{ij} = \hat{Y}_{ij} - Y_{ij}$$

A least squares estimate is used to calculate the coefficients k_0, k_1, and k_2.

$$E = \sum_{\forall ij} e_{ij}^{\,2} = \sum_j \sum_i (k_0 + k_1 X_{ij} + k_2 Z_{ij} - Y_{ij})^2$$

$$\frac{\partial E}{\partial k_0} = 2\sum_j \sum_i (k_0 + k_1 X_{ij} + k_2 Z_{ij} - Y_{ij}) = 0$$

$$\frac{\partial E}{\partial k_1} = 2\sum_j \sum_i (k_0 + k_1 X_{ij} + k_2 Z_{ij} - Y_{ij}) X_{ij} = 0$$

$$\frac{\partial E}{\partial k_2} = 2\sum_j \sum_i (k_0 + k_1 X_{ij} + k_2 Z_{ij} - Y_{ij}) Z_{ij} = 0$$

Using Cramer's rule the following equations for k_0, k_1, and k_2 are calculated. In this solution det is equal to the determinant of A and $NM = \sum_{ij} 1$.

$$Ax = b \rightarrow \begin{bmatrix} NM & \sum_{ij} X_{ij} & \sum_{ij} Z_{ij} \\ \sum_{ij} X_{ij} & \sum_{ij} X_{ij}^{\,2} & \sum_{ij} X_{ij} Z_{ij} \\ \sum_{ij} Z_{ij} & \sum_{ij} X_{ij} Z_{ij} & \sum_{ij} Z_{ij}^{\,2} \end{bmatrix} \begin{bmatrix} k_0 \\ k_1 \\ k_2 \end{bmatrix} = \begin{bmatrix} \sum_{ij} Y_{ij} \\ \sum_{ij} Y_{ij} X_{ij} \\ \sum_{ij} Y_{ij} Z_{ij} \end{bmatrix}$$

$$x = A^{-1} b \rightarrow \begin{bmatrix} k_0 \\ k_1 \\ k_2 \end{bmatrix} = \begin{bmatrix} NM & \sum_{ij} X_{ij} & \sum_{ij} Z_{ij} \\ \sum_{ij} X_{ij} & \sum_{ij} X_{ij}^{\,2} & \sum_{ij} X_{ij} Z_{ij} \\ \sum_{ij} Z_{ij} & \sum_{ij} X_{ij} Z_{ij} & \sum_{ij} Z_{ij}^{\,2} \end{bmatrix}^{-1} \begin{bmatrix} \sum_{ij} Y_{ij} \\ \sum_{ij} Y_{ij} X_{ij} \\ \sum_{ij} Y_{ij} Z_{ij} \end{bmatrix}$$

The following is the solution for each coefficient.

$$k_0 = \frac{\begin{bmatrix} \sum_{ij} Y_{ij} & \sum_{ij} X_{ij} & \sum_{ij} Z_{ij} \\ \sum_{ij} Y_{ij} X_{ij} & \sum_{ij} X_{ij}^2 & \sum_{ij} X_{ij} Z_{ij} \\ \sum_{ij} Y_{ij} Z_{ij} & \sum_{ij} X_{ij} Z_{ij} & \sum_{ij} Z_{ij}^2 \end{bmatrix}}{\det} \quad k_1 = \frac{\begin{bmatrix} NM & \sum_{ij} Y_{ij} & \sum_{ij} Z_{ij} \\ \sum_{ij} X_{ij} & \sum_{ij} Y_{ij} X_{ij} & \sum_{ij} X_{ij} Z_{ij} \\ \sum_{ij} Z_{ij} & \sum_{ij} Y_{ij} Z_{ij} & \sum_{ij} Z_{ij}^2 \end{bmatrix}}{\det} \quad k_2 = \frac{\begin{bmatrix} NM & \sum_{ij} X_{ij} & \sum_{ij} Y_{ij} \\ \sum_{ij} X_{ij} & \sum_{ij} X_{ij}^2 & \sum_{ij} Y_{ij} X_{ij} \\ \sum_{ij} Z_{ij} & \sum_{ij} X_{ij} Z_{ij} & \sum_{ij} Y_{ij} Z_{ij} \end{bmatrix}}{\det}$$

For the spectral differencing experiment we used a 650 nm laser spot source and three optical filters (600 nm, 650 nm, and 700 nm, all with a 40 nm bandwidth). Note that the laser spot frequency is outside the pass bands of the 600 nm, and 700 nm filters. Three images were acquired, one at each band, with the laser on. Then linear interpolation between the 600 nm and 700 nm response was applied to estimate the background in the 650 nm band. Using the above equations the spectral estimate $\hat{Y}$ was calculated where X was the 600 nm filter response, Y was the 650 nm filter response, and Z was the 700 nm filter response. Then differencing was used between the actual 650 nm response Y and the estimate $\hat{Y}$ to subtract out the background clutter and allow segmentation of the laser. The following images demonstrate the ability to extract the laser from background noise.

Figure 14: X = 600 nm Filter Response

Figure 15: Y = 650 nm Filter Response

Figure 16: Z = 700 nm Filter Response

Figure 17: Y_{est} = 650 nm Estimate

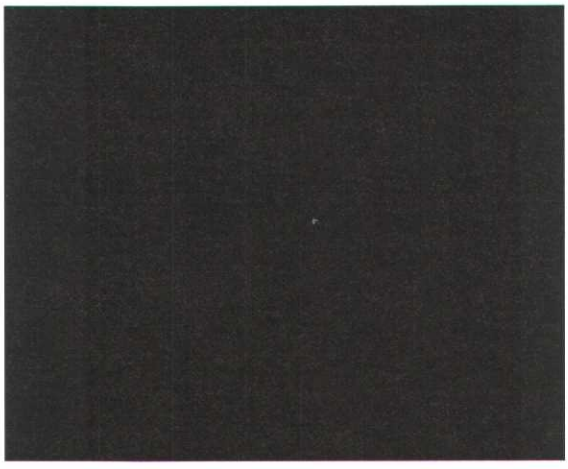

Figure 18: Difference Image

The mean grey level of the 650 nm filter response (Figure 15) was 140.5 with a standard deviation of 44.9. The laser grey level was 255 which is only ~2.56 standard deviations above the mean. For the difference image (Figure 18), the mean grey level was 6.37 with a standard deviation of 5.49. In this image the laser grey level was 121, ~21 standard deviations above the mean.

Laser Pulsing

The last method in consideration was a synchronized laser pulse-width modulation technique that pulses a laser during the open period of the camera shutter. A Class IIIa eye safe laser is limited to 5 mW of continuous optical output power. Pulsing the laser, or decreasing the duty cycle, allows for an increase in the peak power output while remaining eye safe. In addition, if the exposure period of the camera is limited then the background clutter is lowered. The overall effect is an increase in the signal to noise ratio. Modern CCD cameras are equipped with fast shuttering capability (1/100,000 second), high sensitivity (.00015 lux), and allow for manual as well as electronic adjustment of the sensor exposure period.

An experiment was performed to validate the pulsing concept. The laser was viewed using four camera exposure settings or shutter speeds (1/60, 1/120, 1/250, and 1/500 seconds) and four laser power settings. As the exposure was halved, the laser power was doubled to maintain the average power. The following images demonstrate the reduction in background clutter obtained using this technique.

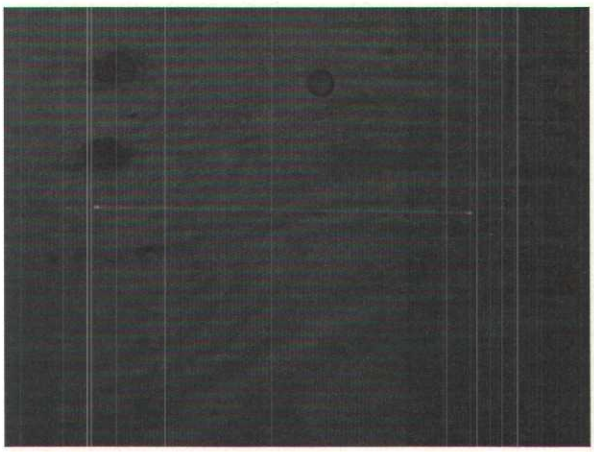

Figure 19: Exposure Period = 1/60 sec
Laser Power = MIN
Mean Grey Level = 49.43
Standard Deviation = 10.48
Laser Grey Level = 58
Laser is ~ .82 std dev above mean

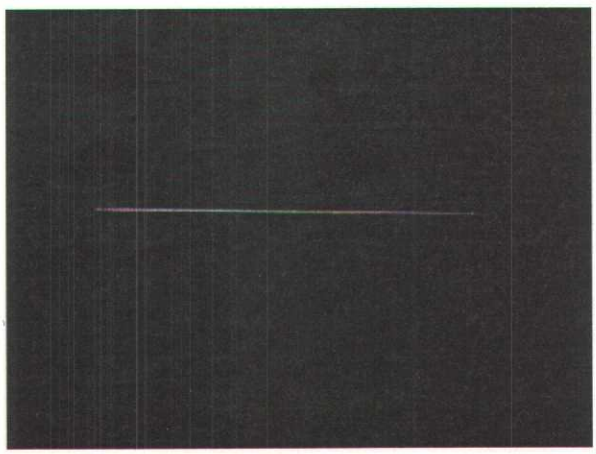

Figure 20: Exposure Period = 1/120 sec
Laser Power = 2 X MIN
Mean Grey Level = 35.67
Standard Deviation = 8.43
Laser Grey Level = 90
Laser is ~ 6.44 std dev above mean

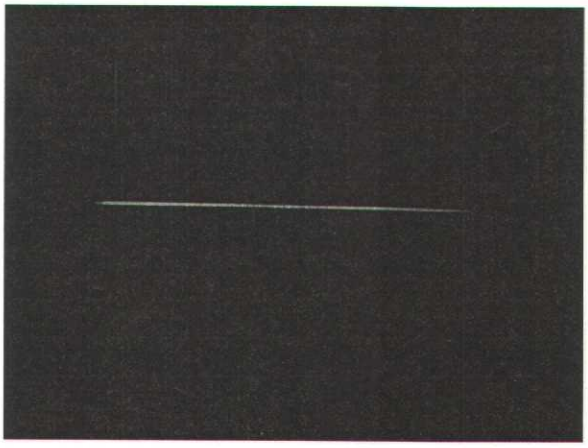

Figure 21: Exposure Period = 1/250 sec
Laser Power = 4 X MIN
Mean Grey Level = 20.06
Standard Deviation = 7.17
Laser Grey Level = 121
Laser is ~ 14.08 std dev above mean

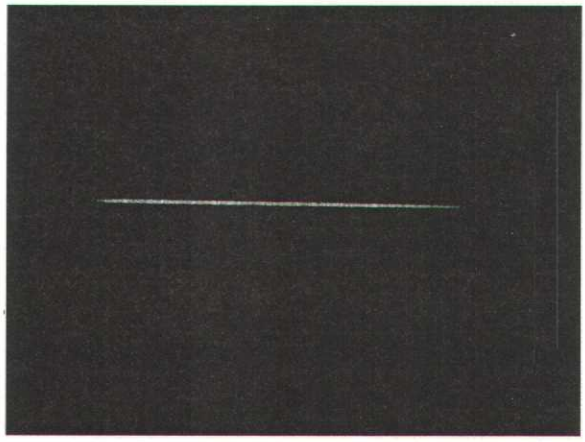

Figure 22: Exposure Period = 1/500 sec
Laser Power = 8 X MIN
Mean Grey Level = 14.43
Standard Deviation = 8.59
Laser Grey Level = 192
Laser is ~ 20.66 std dev above mean

To employ this method, it is necessary to synchronize the laser pulsing with the exposure period of the camera. We used the LM1881 video sync separator to determine when the CCD sensor of the camera was being exposed (i.e. when the shutter was open) during the odd and even fields of each frame. The LM1881 extracts the video sync signal from a standard NTSC camera allowing for the determination of how long after the vertical retrace pulse the camera shutter is open. The timing was determined by pointing the camera directly at an LED that was being pulsed by the MSP430 Texas Instruments microcontroller. The exposure time of the camera was set to 1/250 of a second and the LED was being pulsed for 4 milliseconds. We used the MSP430 to "walk the pulse" along the odd and even fields until the LED showed up in the camera image, thus determining when the shutter was open. Figure 23 illustrates the timing of the laser pulse during the odd and even fields of each frame.

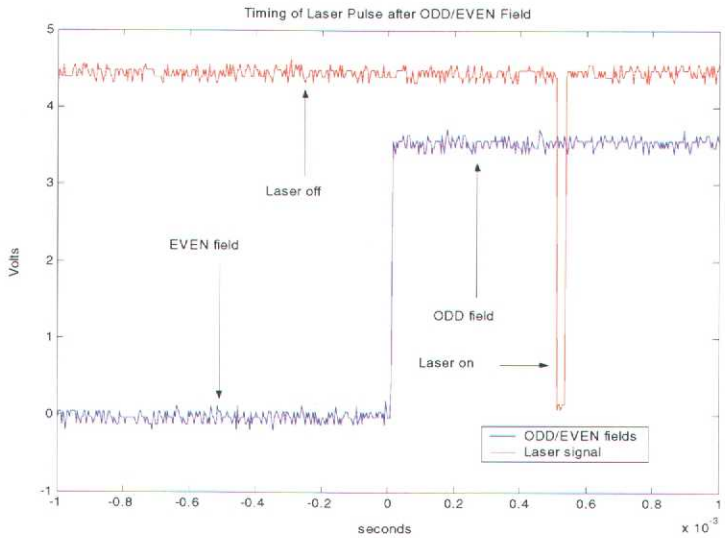

Figure 23: Timing of the Laser Pulse

After determining when the shutter was open, a laser pulsing and hardware interlock safety circuit (Figure 24) was constructed in order to safely pulse the laser. The circuit consists of an LM1881 video sync separator, 74123 retriggerable monostable multivibrator, 7408 AND gate, and a Texas Instrument MSP430 microcontroller. The hardware interlock circuitry assures that the laser is being pulsed for the appropriate duration. Calculations were made, using the American National Standard for Safe Use of Lasers, to determine the maximum pulsed power a continuous wave laser can have for a given pulse duration and still be eye safe at the laser exit. These calculations are based on the wavelength of the laser, the laser geometry, the pulse duration, and the pulse repetition frequency (Appendix A).

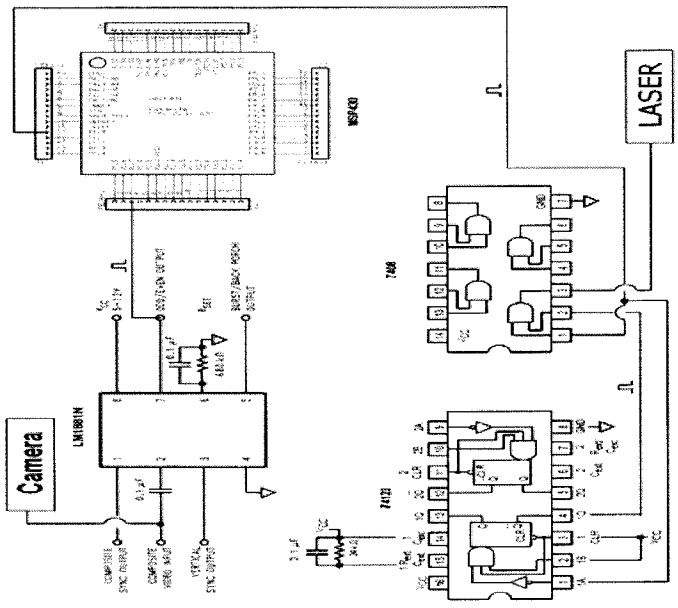

Figure 24: Laser Pulsing and Hardware Interlock Safety Circuit

Conclusion

The results show that polarization can be used successfully to improve the signal to clutter ratio in a structured lighting system for use in outdoor applications. For indoor applications, and considering the surfaces analyzed, the technique seems to have minimal effect. This is due to the large amount of depolarization that takes place in the laser light after reflection and that the background light remains unpolarized after reflection. Although the improvement in the signal to noise ratio may not be sufficient for what is required, the combination of polarization with spectral estimation and pulse-width modulated laser synchronization is. The implementation of such a system is also cost effective. To create a system that can perform in real time on a moving platform, one of two solutions is possible. The first solution is to register the images from three separate synchronized cameras. The second option is to employ Canon's 3CCD color camera technology. This technology uses a prism beam splitter to divide the primary optical path into 3 separate paths with a filter in each path that selects the desired spectral components (Figure 25). We would use our own filters.

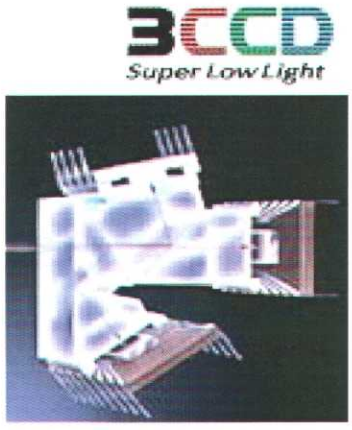

Figure 25: 3CCD Color Camera Technology

Laser pulsing also provides the added benefit of reducing power consumption and size, which is paramount for mobile platforms where space and power are both issues.

Appendix A: Maximum Average Output Power for a Class I Laser

Determination of the maximum average power a CW-IR Diode Laser can have and still be "Class 1" (eye safe) at the laser exit for the following laser operational parameters:

$\lambda = 650$ nm
$t = 10$ μs
PRF = 30 Hz
$D_o \leq 0.7$ cm

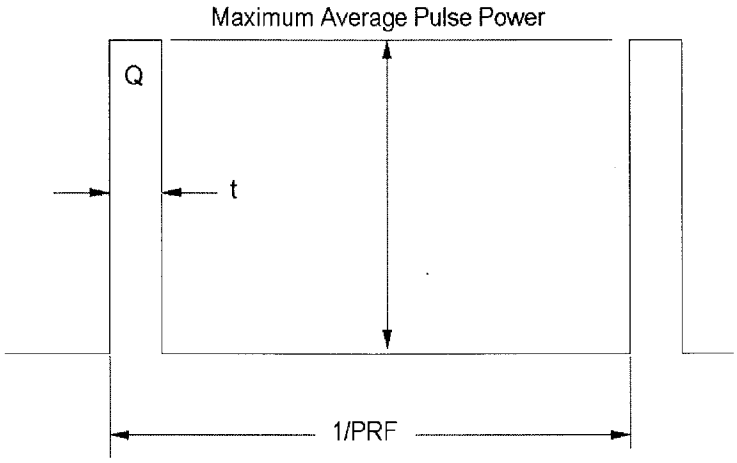

A. **30 Hz PRF**:

1. Determination of the appropriate **Maximum Permissible Exposure** (MPE) for repetitively pulsed lasers.

$$MPE = \min\left|MPE_{rule1}, MPE_{rule2}, MPE_{rule3}\right|$$ ANSI Std. Z136.1-2000 (8.2.3.2)

Rule 1 (Single Pulse):

ANSI Std. Z136.1-2000 (Table 5a)

$$MPE_{rule1} = 5\times10^{-7}\ J/cm^2$$

$400nm < \lambda < 700nm$

$1ns \leq t \leq 18\mu s$

$$MPE_{rule1} = 5\times10^{-7}\ J/cm^2$$

Rule 2 (Average Power over T exposure):

$T \equiv .25\,\text{sec}$ ANSI Std. Z136.1-2000 (Table 4a)

$$MPE_{rule2} = \frac{MPE_{CW} \cdot T}{n} = \frac{MPE_{CW} \cdot T}{PRF \cdot T} = \frac{MPE_{CW}}{PRF}$$

ANSI Std. Z136.1-2000 (Table 5a)

$$MPE_{CW} = 1.8t^{0.75} \times 10^{-3} \, {}^{w}/_{cm^2}$$

$$700nm < \lambda < 1050nm$$

$$18 \times 10^{-6} \sec \le T \le 10 \sec$$

$$MPE_{CW} = .636 \times 10^{-3} \, {}^{w}/_{cm^2}$$

$$MPE_{rule2} = \frac{.636 \times 10^{-3} \, {}^{J}/_{\sec}/_{cm^2}}{30 \sec^{-1}}$$

$$MPE_{rule2} = 21 \times 10^{-6} \, {}^{J}/_{cm^2}$$

Rule 3 (Multiple-Pulse):

$$MPE_{rule3} = C_p \cdot MPE_{rule1}$$

The Determination of the **multiple pulse correction** factor (C_p):

ANSI Std. Z136.1-2000 (Table 6)

$$C_p = n^{-0.25} = [PRF \cdot T]^{-0.25}$$
$$= \left[\left(30 \sec^{-1}\right)(.25 \sec)\right]^{-0.25} = (7.5)^{-0.25}$$

$$C_p = 0.604$$

$$MPE_{rule3} = (0.604)\left(5 \times 10^{-7} \, {}^{J}/_{cm^2}\right)$$

$$MPE_{rule3} = 3.02 \times 10^{-7} \, {}^{J}/_{cm^2}$$

Appropriate MPE:

$$MPE = \min\begin{bmatrix} 5\times10^{-7}\,J/cm^2 \\ 21\times10^{-6}\,J/cm^2 \\ 3.02\times10^{-7}\,J/cm^2 \end{bmatrix} = 3.02\times10^{-7}\,J/cm^2$$

2. Determination of the **Allowable Exposure/Emission Limit** (AEL).

$$AEL = MPE \cdot A_{\lim} = MPE\,\frac{\pi}{4}(d_{\lim})^2$$ ANSI Std. Z136.1-2000 [3.2.3.4.1(2)]

Limiting Aperture ($d_{\lim}$)

$$d_{\lim} = 0.7cm$$ ANSI Std. Z136.1-2000 (Table 8)

$$A_{\lim} = \frac{\pi}{4}(0.7cm)^2 = 0.385cm^2$$

$$AEL_{60Hz} = \left(3.02\times10^{-7}\,J/cm^2\right)\left(0.385cm^2\right)$$

$$AEL_{60Hz} = 116.3\times10^{-9}\,J$$

3. Determination for the **Maximum Average Pulse Power** (Φ) for Class 1 operation.

The average pulse power is the total energy of the pulse (Q) divided by the pulse duration (t).

$$\Phi = \frac{Q}{t}$$

The average pulse power for a one-microsecond pulse at 30 hertz is determined as follows;

t = 10 μs:

$$\Phi_{10\mu s} = \frac{AEL}{t} = \frac{116.3\times10^{-9}\,J}{10\times10^{-6}\,\text{sec}}$$

$$\Phi_{10\mu s} = 11.6\times10^{-3}\,watts$$

B. **For Beams Larger Than The Limiting Aperture.**

Example Presented in paper:

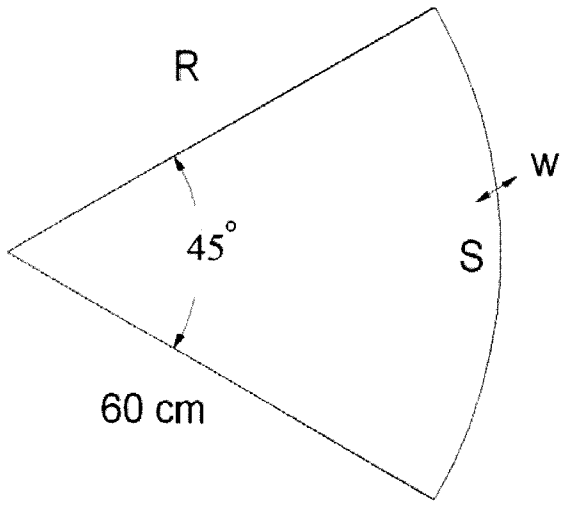

Fan angle is 45° (one direction)
Beam width is 0.7 cm (other direction)
Minimum viewing distance (engineering control) is 60 cm.

The length of the arc (S_{60cm}) can be calculated as:

$$S_R = \theta \cdot R$$

Where, $\theta = (45^{\circ})\frac{\pi}{180^{\circ}} = \frac{\pi}{4}$,

and $R = 60cm$

$$S_{60cm} = \frac{\pi}{4} \cdot 60cm = 15\pi \ cm$$

The illuminated area at the minimum viewing distance is:

$$A = S \cdot w$$

$$A_{60cm} = \frac{\pi}{4} \cdot 60cm \cdot 0.7cm$$

$$A_{60cm} = 10.5\pi \ cm^2$$

The maximum energy that can be deposited in this area and still be Class 1 eye safe is:

$$Q_{\max-60cm} = MPE \cdot A_{60cm}$$

$$Q_{\max-60cm} = \left(302\times10^{-9} \, J/cm^2\right)\left(10.5\pi \ cm^2\right)$$

$$Q_{\max-60cm} = 9.96\times10^{-6} J$$

The maximum pulse average power for one-microsecond pulse at 30 hertz is:

$$\Phi_{\max-60cm} = \frac{Q_{\max-60cm}}{1\mu s} = \frac{9.96\times10^{-6} J}{10^{-6} \sec} = 9.96 \ \ watts$$

The maximum pulse average power for ten-microsecond pulse at 30 hertz is:

$$\Phi_{\max-60cm} = \frac{Q_{\max-60cm}}{10\mu s} = \frac{10.2\times10^{-6} J}{10\times10^{-6} \sec} = 1.02 \ \ watts$$

References

[1] C. Mertz, J. Kozar, J.R. Miller, and C. Thorpe, *Eye-safe Laser Line Striper for Outside Use*, CMU, Robotics Institue (2001).

[2] B.K.P. Horn, *Robot Vision*, MIT Press, Cambridge, MA (1986).

[3] P.J. Besl, Active, Optical Imaging Sensors, *Machine Vision and Applications*, Vol. 1, pp. 127-152 (1988)

[4] E. Krotkow, Focusing, International Journal of Computer Vision, Vol. 1, pp. 223-238 (1987)

[5] S. T. Barnard, and W. B. Thompson, "Disparity analysis of images", *IEEE Trans. Pattern Anal. Mach. Intell*, 1980, 2(4), 333-340.

[6] G. Kylberg, "Measurement of interference fringe separation by a moire technique"The Institute of Optical Research, Stockholm, Sweden *1968*

[7] Horvart, Gabor and Varju Dezso. "Polarized light in animal vision". Springer, 2004.

[8] Hecht, E., "Optics". Addison Wesley, fourth edition, 2002

[9] Konnen, G. P. "Polarized light in nature". Cambridge University Press, 1985.

[10] Schott, John R., "Remote Sensing - the image chain approach", Oxford University Press, NY, 1997.

[11] Clémenceau, P. et al. "Polarization active imaging". Proc. SPIE Vol. 4035, p. 401-409, Laser Radar Technology and Applications, 2000.

[12] Clémenceau, P. et al. "Modeling and performances of a polarization active imager at λ = 806 nm. Optical Engineering". Volume 39, Issue 10, pp. 2681-2688, 2000.

[13] Miyazaki, D. et al. "Determining surface orientation of transparent objects based on polarization degrees in visible and infrared wavelengths". Optical Society of America, Vol. 19, No. 4, 2002.

[14] Bueno, J. M."Degree of polarization as an objective method of estimating scattering". JOSA A, Volume 21, Issue 7, 1316-1321, 2004.

[15] Wolf, L. "Liquid Crystal Polarization Camera". Proc. SPIE Vol. 1823, p. 102-113, Machine Vision Applications, Architectures, and Systems Integration, 1992.

[16] Andreou, A. G. and Kalayjian, Z. K., "Polarization imaging: principles and integrate polarimeters". IEEE Sensors Journal, Vol. 2, No. 6, pp. 566-576 2002

[17] Woff, L. "Applications of polarization camera technology". IEEE Expert, October, 1995.

[18] Konnen, G. P. "Polarized light in nature". Cambridge University Press, 1985.

[19] Shurcliff, W. "Polarized Light". Howard University Press, 1962.

[20] Huard, S. Polarization of light.

[21] Odom, B. W. "Liquid crystal variable retarder based imaging polarimeter". New Mexico State Unversity – Electro-optics department, master thesis, 2004.

[22] Bruce, N. C. "Calculations of the Mueller matrix for scattering light from two-dimensional surfaces". Waves in random media 8, 15-28, 1998.

[23] Goudail, F and Réfrégier, P. "Statistical algorithms for target detection in coherent active polarimetric images". Optical Society of America Journal, Volume 18, Issue 12, pp. 3049-3060, 2001.

Distribution

1	MS 0123	D. L. Chavez 01011
1	MS 1002	S. C. Roehrig 06600
1	MS 1003	J. T. Feddema 06634
5	MS 1003	D. D. Padilla 06646
1	MS 1003	J. J. Carlson 06646
1	MS 1010	C. H. Duus Jr. 06646
1	MS 1003	D. K. Novick 06646
1	MS 1003	P. A. Davidson Jr. 06646
6	MS 1003	B. Ewing 06634
6	MS 1010	S. K. Willis 06633
2	MS 9018	Central Technical Files, 8945-1
2	MS 0899	Technical Library, 4536